JACS
JOURNAL OF THE AMERICAN CHEMICAL SOCIETY
Communication
pubs.acs.org/JACS

$Ca_2Mn_2O_5$ as Oxygen-Deficient Perovskite Electrocatalyst for Oxygen Evolution Reaction

Jaemin Kim, Xi Yin, Kai-Chieh Tsao, Shaohua Fang, and Hong Yang*

Department of Chemical and Biomolecular Engineering, University of Illinois at Urbana−Champaign, 114 Roger Adams Laboratory, MC-712, 600 South Mathews Avenue, Urbana, Illinois 61801, United States

Supporting Information

ABSTRACT: This paper presents the use of $Ca_2Mn_2O_5$ as an oxygen-deficient perovskite electrocatalyst for oxygen evolution reaction (OER) in alkaline media. Phase-pure $Ca_2Mn_2O_5$ was made under mild reaction temperatures through a reductive annealing method. This oxygen deficient perovskite can catalyze the generation of oxygen at ∼1.50 V versus (vs) reversible hydrogen electrode (RHE) electrochemically, and reach an OER mass activity of 30.1 A/g at 1.70 V (vs RHE). In comparison to the perovskite $CaMnO_3$, $Ca_2Mn_2O_5$ shows higher OER activities. The molecular level oxygen vacancies and high spin electron configuration on manganese in the crystal structures are likely the contributing factors for the enhanced performance. This work demonstrates that oxygen-deficient perovskite, $A_2B_2O_5$, is a new class of high performance electrocatalyst for those reactions that involve active oxygen intermediates, such as reduction of oxygen and OER in water splitting.

Various perovskites and their related structures have rapidly emerged as promising, highly efficient active materials for applications in solar cell,[1−3] water splitting device[4] and metal air battery.[5,6] The known perovskites include organometallic halide[7,8] and inorganic compounds. An important advantage on using perovskites in such these applications, besides the economic benefit by avoiding the use of noble metals, is their flexibility in composition, thus the electronic structures of catalysts. In an ABX_3 (or ABO_3)-type perovskite structure, both A- and B-sites can vary systematically using metal cations with different valences or ionic radii. Partial replacement or doping at these sites is also relatively straightforward and results in a systematic change of chemical, electronic, and physical properties. For the past several years, a series of perovskites were intensively studied as electrocatalysts for oxygen reduction reaction (ORR) and oxygen evolution reaction (OER)[9−11] since Bockris et al. reported the intrinsic electrocatalytic activities of perovskite oxides.[12,13] The e_g-filling status of B-site metal ions (e.g., Mn, Ni, and Co) of the perovskites was considered to be critical for high electrocatalytic activities in OER based on both the experimental data and theoretical analysis of the electronic structures of molecular orbitals.

Besides composition, nanostructure is also considered to be important for electrocatalytic performance. In this regard, pyrochlores with mesoporous structure were examined as catalysts for lithium−oxygen batteries. The nanocrystalline pyrochlores electrocatalyts showed high yield of discharge capacities and low anodic overpotentials.[14,15] The superior performance is resulted from their high fraction of surface defect sites with the unique porous morphology and variable oxygen stoichiometry. Thus, it is interesting to examine the electrocatalytic performance of those perovskite-related oxides that have ordered defects in their crystal structures. In this context, although a series of studies have been done with perovskites, the electrocatalytic performance of ordered oxygen-deficient perovskite, especially those with molecular level porosity such as $Ca_2Mn_2O_5$ (or $CaMnO_{2.5}$), have not been carried out yet. There has been no careful examination of OER or ORR activities on these types of oxides directly or indirectly. In this paper, we present a new low-temperature synthesis and OER property of $Ca_2Mn_2O_5$ and compare its electrocatalytic activity with the perovskite-type $CaMnO_3$.

One crystal structure for $Ca_2Mn_2O_5$ (or $CaMnO_{2.5}$) and two for $CaMnO_3$ are known; namely, orthorhombic (*Pbam*) $CaMnO_{2.5}$, and cubic ($Pm\bar{3}m$) and orthorhombic (*Pnma*) perovskite $CaMnO_3$. We have chosen orthorhombic structures for both types of metal oxides and compared their OER activities directly. Both $CaMnO_x$ (x = 2.5 and 3) have the same atomic arrangement, except the oxygen-defect sites in the crystal structures. The orthorhombic $Ca_2Mn_2O_5$ has five-coordinated square pyramid subunits between manganese and oxygen, in which all five oxygen atoms are linked with adjacent subunits through corner oxygen atoms. The orthorhombic $CaMnO_3$ has six-coordinated octahedral subunits linked through the six oxygen atoms at the corner sites. Thus, oxygen deficient perovskite $Ca_2Mn_2O_5$ has intrinsic molecular level porosity on the oxygen deficient sites, which are beyond structural porosity, such as mesoporosity or macroporosity. This structure could facilitate ion transport for OER via oxygen vacancies.

Phase pure $Ca_2Mn_2O_5$ was made through the reductive annealing from as-made perovskite $CaMnO_3$ (Figure S1), which was synthesized via a sol−gel process (Scheme 1). Hydrogen gas was used to reduce Mn^{4+} ions in $CaMnO_3$ to

Scheme 1. Synthesis Route for $CaMnO_3$ (*Pnma*) and $Ca_2Mn_2O_5$ (*Pbam*)

Received: June 21, 2014
Published: October 8, 2014

   dx.doi.org/10.1021/ja506254g | J. Am. Chem. Soc. 2014, 136, 14646−14649

Mn^{3+} to form single crystal phase oxygen deficient perovskite $Ca_2Mn_2O_5$ (see Supporting Information for detail).[16] Previous work indicated that oxygen deficient perovskites could be made by introducing reactive metal (oxygen acceptor, such as Zr)[17] or quenching the perovskite from high temperature to room temperature.[18] These methods are not ideal because they are often accompanied by the difficulty with the control of oxygen vacancy in order to obtain phase pure materials. Unlike the quenching method, reductive annealing can be carried out at a relatively low temperature, thus control the kinetics of manganese oxidation states, resulting in single phase $Ca_2Mn_2O_5$. In this study, we developed a new method by using a forming gas of 5% H_2 in Ar. We discovered $Ca_2Mn_2O_5$ could be synthesized from perovskite $CaMnO_3$ at 350 °C for a reaction time of 3 h. This mild solid-state reaction condition allows for both shorter reaction time and lower reaction temperature than other methods.[16,18−21]

Figure 1 shows the powder X-ray diffraction (PXRD) patterns of the as-made $Ca_2Mn_2O_5$. All the diffraction peaks

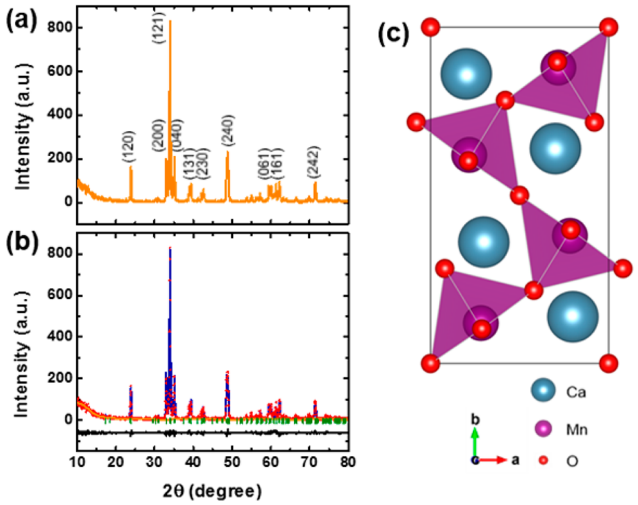

Figure 1. (a) PXRD pattern and (b) Rietveld refinement plot of $Ca_2Mn_2O_5$ (orthorhombic, *Pbam*): experimental data (red), simulated diffraction (blue), background (orange), observed reflections (green), and difference (black). (c) Unit cell of oxygen deficient perovskite $Ca_2Mn_2O_5$, showing the ordered oxygen vacancy along directions normal to the *ab* plane.

could be indexed to orthorhombic (*Pbam*) phase $Ca_2Mn_2O_5$ (JCPDS No. 076−1133) (Figure 1a). The PXRD pattern was further analyzed by the Rietveld refinement method, in which ICCD crystal model and a pseudo-Voigt function were employed for peak profile fitting (Figure 1b, Table S1). The refined lattice parameters were indexed as a = 5.4302(7) Å, b = 10.2311(1) Å and c = 3.7443(2) Å, with less than 0.11% mismatch from the reference XRD pattern, which confirms the single crystalline phase. The discrepancy factors showed a bit high values with R_p = 16.39% and R_{wp} = 10.40%, mainly resulted from the peaks with low intensities (Table S1). The unit cell of the $Ca_2Mn_2O_5$ is shown in Figure 1c. In this unit cell, oxygen atom is missing from octahedral MnO_6 subunit along directions normal to the *ab* plane. The oxygen-deficient structure gives a square pyramid MnO_5 subunit with a zigzag structure, resulting in the internal molecular level porosity on $Ca_2Mn_2O_5$.

Figure 2 shows the scanning electron microscope (SEM) and the high resolution transmission electron microscope

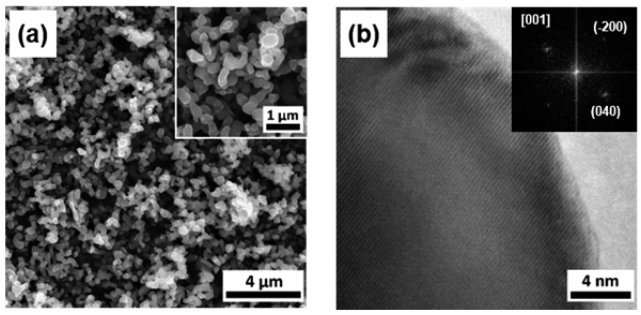

Figure 2. (a) SEM, and (b) HRTEM and FFT (inset) images of $Ca_2Mn_2O_5$ with submicron-sized particles. The inset of (a) is a magnified image.

(HRTEM) images of the $Ca_2Mn_2O_5$. The average particle size is less than 1 μm (Figure 2a), showing the fine powder form with similar particle size for as-made $CaMnO_3$ (Figure S2). No sintering or coalescence was observed after the conversion, showing the advantage of this low-temperature, reductive annealing approach in the synthesis of oxide catalysts. The reaction time did not seem to be critical for maintaining the morphology. One of the advantages of sol−gel process over the more traditional solid-state synthesis is that it can reduce the reaction temperature without generating mixed phases due to the decreased ions diffusion path lengths. The chelating agent such as citric acid helps the even distribution of various precursors at molecular level, which results in small particle sizes at relatively low temperature.[22] The reductive annealing did not result in obvious sintering of the particles. Figure 2b shows the representative HRTEM image of the single crystalline structure of orthorhombic $Ca_2Mn_2O_5$. The crystallinity is high and lattice fringes are clearly visible from center to surface of the particle. The inset shows the fast Fourier transform (FFT) analysis of the HRTEM image, further confirms the orthorhombic structure of $Ca_2Mn_2O_5$.

We evaluated the OER activities of $Ca_2Mn_2O_5$ and $CaMnO_3$ in O_2-saturated 0.1 M KOH solution. Before each measurement, the potential for reversible hydrogen electrode (RHE) was calibrated using a platinum working electrode under the hydrogen gas-saturated solution. The electrolyte resistance under the oxygen gas was measured to be about 50 Ω for the same electrolyte solution to ensure the accuracy. Freshly prepared metal oxide catalysts ink was deposited on glassy carbon rotating disk electrodes (RDEs). All data were collected within 4 h to minimize any side reactions. Cyclic voltammograms (CVs) rather than linear sweep voltammograms (LSVs) were obtained at 1600 rpm under ambient room temperature to obtain OER currents. The scan rate was set at 10 mV/s and the scan range was from 1.1 to 1.8 V. Three independent OER measurements were carried out for each catalyst. The collected data were corrected for the capacitance and *iR*. Figure 3a shows the *iR*-corrected CV data of $Ca_2Mn_2O_5$/C, $CaMnO_3$/C and Vulcan carbon XC-72. The carbon support had no measurable contribution to the current for either $Ca_2Mn_2O_5$/C or $CaMnO_3$/C in the measured potential range. The onset currents started at ∼1.50 V for both positive and negative scans for the oxygen deficient perovskite $Ca_2Mn_2O_5$/C, showing a lower overpotential (η = ∼0.1 V) than $CaMnO_3$/C (∼1.60 V). The onset potential of $Ca_2Mn_2O_5$/C is also

dx.doi.org/10.1021/ja506254g | J. Am. Chem. Soc. 2014, 136, 14646−14649

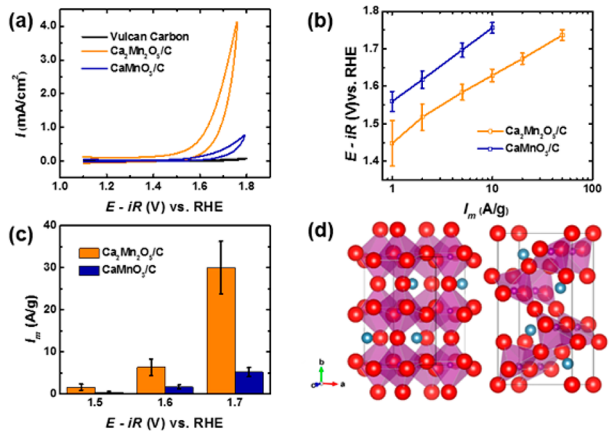

Figure 3. (a) *iR*-corrected data of $Ca_2Mn_2O_5$/C, $CaMnO_3$/C, and Vulcan carbon XC-72, (b) Tafel plot of mass activities (error bars represents standard deviations from three independent measurements), and (c) mass activities at various applied potentials. (d) Unit cell structures of $CaMnO_3$ (left) and $Ca_2Mn_2O_5$ (right).

competitive with the state-of-the-art highly active OER catalysts, such as RuO_2 (~1.45 V), IrO_2 (~1.50 V) and $Pr_{0.5}Ba_{0.5}CoO_{3-\delta}$ (~1.45 V).[9,11,23] It needs to be mentioned that hysteresis was found for both perovskite oxide catalysts over the CVs,[9] presumably due to partial degradation of the catalysts at applied high potentials (Figure S3).[24]

A rotating ring disk electrode (RRDE) study was carried out to examine the origin of the observed currents (Figure S4). The applied potential was set to 1.60 and 1.80 V on glassy carbon disk electrode for the oxidation process ($4OH^- \rightarrow O_2 + 2H_2O + 4e^-$), and 0.40 V was applied to the Pt-ring electrode for the reduction process ($O_2 + 2H_2O + 4e^- \rightarrow 4OH^-$). The reduction currents at Pt-ring electrode depended strongly on the oxidation currents on disk with initial high currents, confirming the OER process occurred for both $CaMnO_x$ electrocatalysts.[23] Figure 3b shows the Tafel plot of OER mass activities for the capacitance- and *iR*-corrected average CVs of $Ca_2Mn_2O_5$/C and $CaMnO_3$/C, respectively. The OER mass activities of oxygen deficient perovskite $Ca_2Mn_2O_5$/C is higher than perovskite $CaMnO_3$/C throughout all the applied potential range. The difference in mass activity between the two oxides becomes larger at high potential ranges. The Tafel slopes for $Ca_2Mn_2O_5$/C and $CaMnO_3$/C are 149 and 197 mV/dec, respectively, which agree with the literature values (Figure S5).[25,26] Figure 3c compares the OER mass activities at specific applied potentials. It is noteworthy that OER mass activity of $Ca_2Mn_2O_5$/C is about 4–6 times higher than $CaMnO_3$/C through all the applied potentials; 1.64 A/g for $Ca_2Mn_2O_5$ and 0.47 A/g for $CaMnO_3$ at 1.50 V, 6.39 A/g for $Ca_2Mn_2O_5$ and 1.66 A/g for $CaMnO_3$ at 1.60 V, and 30.07 A/g for $Ca_2Mn_2O_5$ and 5.19 A/g for $CaMnO_3$ at 1.70 V. Figure 3d shows the unit cell structures for $CaMnO_3$ and $Ca_2Mn_2O_5$, respectively. The ionic radii are 0.99 Å for Ca^{2+}, 1.4 Å for O^{2-}, 0.645 Å for Mn^{3+}, and 0.53 Å for Mn^{4+}.[27] Direct comparison of these two structures shows bonding of OH^- occurs more readily to MnO_5 subunit in $Ca_2Mn_2O_5$ than fully coordinated MnO_6 subunit in $CaMnO_3$.[13,28]

Removing the lattice oxygen from perovskite creates oxygen-deficient structure. This structural change should result in differences in electrocatalytic performance depending on the existence of the oxygen vacancies in the structures. For $CaMnO_x$ compounds, removal of oxygen atoms from $CaMnO_3$ resulted in the change in unit cell structure as well as electron configuration on manganese, and molecular level porous structure in oxygen deficient perovskite $Ca_2Mn_2O_5$. First, relatively large ion radius of Mn^{3+} (0.645 Å, high spin) in $Ca_2Mn_2O_5$ compared to Mn^{4+} (0.53 Å) in $CaMnO_3$, can induce a low tolerance factor, *t*, deviated from unity based on the following equation:[22,29]

$$t = (r_A + r_O)/\sqrt{2}(r_B + r_O)$$

where r_A, r_B, and r_O are the radii of A, B and O ions, respectively. A low *t* value means increased structural distortion. This low *t* value and the Jahn–Teller effect result in more distorted structure and larger cell volume for this oxygen deficient perovskite structure than that from simple stacking of two unit cells of perovskite $CaMnO_3$.[30] The refined cell parameters of $Ca_2Mn_2O_5$ (Table S1) show the unit cell structure elongates in *b*- and *c*-directions preferentially. This distortion arising from oxygen vacancies should help OH^- ion uptake into the oxygen vacant sites.[31−33] Electronic configuration of Mn^{3+} ($3d^4$) in $Ca_2Mn_2O_5$ gives $t_{2g}^3\ e_g^1$ configuration, the high spin state on manganese.[16,20,34−38] This high spin state orbital with e_g^1 electron in manganese can be pointed toward OH^- ion, giving high OER activity.[11] The perovskite structure of $CaMnO_3$, on the other hand, has Mn^{4+} ($3d^3$) with t_{2g}^3 electronic configuration, which cannot easily form bonding structure with OH^-, thus showing a lower OER activity than $Ca_2Mn_2O_5$. $Ca_2Mn_2O_5$ also possess oxygen defect sites, in which the oxygen vacancies give the ordered structure and the molecular level oxygen porosity beyond the mesoscale porosity. Thus, this oxygen vacant site should assist the adsorption of OH^-, leading to the fast OER kinetics.

The exchange between O^{2-} and O_2^{2-} species is considered to be the rate-determining step for the OER cycle, a hypothesis that is supported by theoretical models and experimental data.[11] On the basis of this reaction mechanism, the kinetic of both OH^- bonding via the oxygen vacant site on MnO_5 subunit and the above step of ion exchange need to be taken into the consideration, because once OH^- binds to manganese ofMnO_5 unit ER cycle starts. Figure 4 depicts a plausible effect of oxygen

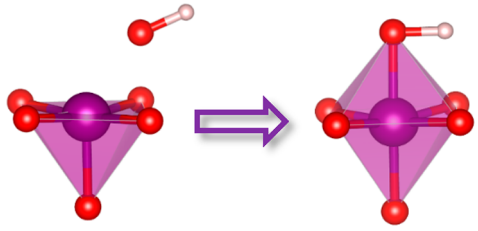

Figure 4. Illustration of possible effect of oxygen vacancy in the $Ca_2Mn_2O_5$ crystal structure on oxygen evolution kinetics.

vacancy on the reaction kinetics within the orthorhombic $Ca_2Mn_2O_5$ structure based on the analysis of the experimental data. OH^- species should adsorb readily on the oxygen vacant site of MnO_5 subunit because of the structure that facilitates ion transport, in which e_g orbital on Mn^{3+} and the O-p_σ orbital on OH^- are overlapping,[10] leading to the formation of intermediate of OH^--MnO_5 octahedral unit.[13] The moderate bonding strength by overlapping of two orbitals also facilitates the ion exchange, i.e., the rate determining step in the OER cycle,[11] resulting in faster OER kinetics with lower over-

dx.doi.org/10.1021/ja506254g | J. Am. Chem. Soc. 2014, 136, 14646−14649

potential on oxygen gas evolution and higher mass activity than perovskite $CaMnO_3$.

In conclusion, we developed a new method for making orthorhombic $Ca_2Mn_2O_5$ from perovskite $CaMnO_3$ through a facile reductive annealing process at low temperature without obvious particle sintering at the submicron size scale. This oxygen deficient perovskite ($A_2B_2O_5$) structure has corner-linked square-pyramidal MnO_5 subunits, resulting in molecular level porosity due to the oxygen vacancy. The oxygen deficient perovskite $Ca_2Mn_2O_5$ has an OER activity that is higher than that of perovskite $CaMnO_3$. This high OER performance could be the result of (1) unit cell structure favoring the facile transport of OH^- ion, (2) electronic configuration of manganese cation (B-site) with high spin electron occupying e_g orbitals, and (3) easy bonding formation between Mn^{3+} and OH^- through oxygen vacancy. Thus, oxygen deficient perovskite ($A_2B_2O_5$) represents a new class of property-tunable oxides for designing cost-effective and high performance catalysts and electrocatalysts without the use of precious metals.

■ ASSOCIATED CONTENT

Ⓢ Supporting Information

Experimental details, detailed Rietveld analysis data, TEM images, SEM images, RRDE graphs, cyclic voltammograms. This material is available free of charge via the Internet at http://pubs.acs.org.

■ AUTHOR INFORMATION

Corresponding Author

hy66@illinois.edu

Notes

A provisional patent is filed based on this research work.

■ ACKNOWLEDGMENTS

This work was supported by a start-up fund from University of Illinois.

■ REFERENCES

(1) Lee, M. M.; Teuscher, J.; Miyasaka, T.; Murakami, T. N.; Snaith, H. J. *Science* **2012**, *338*, 643.
(2) Liu, M. Z.; Johnston, M. B.; Snaith, H. J. *Nature* **2013**, *501*, 395.
(3) Loi, M. A.; Hummelen, J. C. *Nat. Mater.* **2013**, *12*, 1087.
(4) Vojvodic, A.; Norskov, J. K. *Science* **2011**, *334*, 1355.
(5) Hardin, W. G.; Slanac, D. A.; Wang, X.; Dai, S.; Johnston, K. P.; Stevenson, K. J. *J. Phys. Chem. Lett.* **2013**, *4*, 1254.
(6) Takeguchi, T.; Yamanaka, T.; Takahashi, H.; Watanabe, H.; Kuroki, T.; Nakanishi, H.; Orikasa, Y.; Uchimoto, Y.; Takano, H.; Ohguri, N.; Matsuda, M.; Murota, T.; Uosaki, K.; Ueda, W. *J. Am. Chem. Soc.* **2013**, *135*, 11125.
(7) Mitzi, D. B. In *Progress in Inorganic Chemistry*; Karlin, K. D., Ed.; Wiley: New York, 1999; Vol. *48*, p 1.
(8) Park, N. G. *J. Phys. Chem. Lett.* **2013**, *4*, 2423.
(9) Grimaud, A.; May, K. J.; Carlton, C. E.; Lee, Y. L.; Risch, M.; Hong, W. T.; Zhou, J. G.; Shao-Horn, Y. *Nat. Commun.* **2013**, *4*, 2439.
(10) Suntivich, J.; Gasteiger, H. A.; Yabuuchi, N.; Nakanishi, H.; Goodenough, J. B.; Shao-Horn, Y. *Nat. Chem.* **2011**, *3*, 647.
(11) Suntivich, J.; May, K. J.; Gasteiger, H. A.; Goodenough, J. B.; Shao-Horn, Y. *Science* **2011**, *334*, 1383.
(12) Bockris, J. O.; Otagawa, T. *J. Phys. Chem.* **1983**, *87*, 2960.
(13) Bockris, J. O.; Otagawa, T. *J. Electrochem. Soc.* **1984**, *131*, 290.
(14) Oh, S. H.; Black, R.; Pomerantseva, E.; Lee, J. H.; Nazar, L. F. *Nat. Chem.* **2012**, *4*, 1004.
(15) Oh, S. H.; Nazar, L. F. *Adv. Energy Mater.* **2012**, *2*, 903.
(16) Poeppelmeier, K. R.; Leonowicz, M. E.; Scanlon, J. C.; Longo, J. M.; Yelon, W. B. *J. Solid State Chem.* **1982**, *45*, 71.
(17) Caignaert, V. *J. Magn. Magn. Mater.* **1997**, *166*, 117.
(18) Zeng, Z.; Greenblatt, M.; Croft, M. *Phys. Rev. B: Condens. Matter Mater. Phys.* **1999**, *59*, 8784.
(19) Zotzl, M.; Pollmann, H. *J. Am. Ceram. Soc.* **2006**, *89*, 3491.
(20) Zampieri, G.; Prado, F.; Caneiro, A.; Briatico, J.; Causa, M. T.; Tovar, M.; Alascio, B.; Abbate, M.; Morikawa, E. *Phys. Rev. B: Condens. Matter Mater. Phys.* **1998**, *58*, 3755.
(21) Poeppelmeier, K. R.; Leonowicz, M. E.; Longo, J. M. *J. Solid State Chem.* **1982**, *44*, 89.
(22) Jorge, M. E. M.; dos Santos, A. C.; Nunes, M. R. *Int. J. Inorg. Mater.* **2001**, *3*, 915.
(23) Lee, Y.; Suntivich, J.; May, K. J.; Perry, E. E.; Shao-Horn, Y. *J. Phys. Chem. Lett.* **2012**, *3*, 399.
(24) Messaoudi, B.; Joiret, S.; Keddam, M.; Takenouti, H. *Electrochim. Acta* **2001**, *46*, 2487.
(25) Hardin, W. G.; Mefford, J. T.; Slanac, D. A.; Patel, B. B.; Wang, X.; Dai, S.; Zhao, X.; Ruoff, R. S.; Johnston, K. P.; Stevenson, K. J. *Chem. Mater.* **2014**, *26*, 3368.
(26) Matsumoto, Y.; Sato, E. *Electrochim. Acta* **1979**, *24*, 421.
(27) Shannon, R. D. *Acta Crystallogr., Sect. A: Found. Crystallogr.* **1976**, *32*, 751.
(28) Oh, T. S.; Boyd, D. A.; Goodwin, D. G.; Haile, S. M. *Phys. Chem. Chem. Phys.* **2013**, *15*, 2466.
(29) Sousa, D.; Nunes, M. R.; Silveira, C.; Matos, I.; Lopes, A. B.; Jorge, M. E. M. *Mater. Chem. Phys.* **2008**, *109*, 311.
(30) Abakumov, A. M.; Rozova, M. G.; Antipov, E. V. *Usp. Khim.* **2004**, *73*, 917.
(31) Zhang, G. B.; Smyth, D. M. *Solid State Ionics* **1995**, *82*, 161.
(32) Zhang, G. B.; Smyth, D. M. *Solid State Ionics* **1995**, *82*, 153.
(33) Yamazaki, Y.; Babilo, P.; Haile, S. M. *Chem. Mater.* **2008**, *20*, 6352.
(34) Mori, T.; Inoue, K.; Kamegashira, N.; Yamaguchi, Y.; Ohoyama, K. *J. Alloys Compd.* **2000**, *296*, 92.
(35) Matar, S. F.; Etourneau, J. *Int. J. Inorg. Mater.* **2000**, *2*, 523.
(36) Matar, S. F. *Solid State Sci.* **2002**, *4*, 1265.
(37) Maitra, U.; Naidu, B. S.; Govindaraj, A.; Rao, C. N. R. *Proc. Natl. Acad. Sci. U. S. A.* **2013**, *110*, 11704.
(38) Kruth, A.; West, A. R. *J. Mater. Chem.* **2001**, *11*, 153.